Protein disulfide isomerase inhibitors constitute a new class of antithrombotic agents

Reema Jasuja, Freda H. Passam, Daniel R. Kennedy, Sarah H. Kim, Lotte van Hessem, Lin Lin, Sheryl R. Bowley, Sucharit S. Joshi, James R. Dilks, Bruce Furie, Barbara C. Furie, and Robert Flaumenhaft

Division of Hemostasis and Thrombosis, Department of Medicine, Beth Israel Deaconess Medical Center, Harvard Medical School, Boston, Massachusetts, USA.

Thrombosis, or blood clot formation, and its sequelae remain a leading cause of morbidity and mortality, and recurrent thrombosis is common despite current optimal therapy. Protein disulfide isomerase (PDI) is an oxidoreductase that has recently been shown to participate in thrombus formation. While currently available antithrombotic agents inhibit either platelet aggregation or fibrin generation, inhibition of secreted PDI blocks the earliest stages of thrombus formation, suppressing both pathways. Here, we explored extracellular PDI as an alternative target of antithrombotic therapy. A high-throughput screen identified quercetin-3-rutinoside as an inhibitor of PDI reductase activity in vitro. Inhibition of PDI was selective, as quercetin-3-rutinoside failed to inhibit the reductase activity of several other thiol isomerases found in the vasculature. Cellular assays showed that quercetin-3-rutinoside inhibited aggregation of human and mouse platelets and endothelial cell–mediated fibrin generation in human endothelial cells. Using intravital microscopy in mice, we demonstrated that quercetin-3-rutinoside blocks thrombus formation in vivo by inhibiting PDI. Infusion of recombinant PDI reversed the antithrombotic effect of quercetin-3-rutinoside. Thus, PDI is a viable target for small molecule inhibition of thrombus formation, and its inhibition may prove to be a useful adjunct in refractory thrombotic diseases that are not controlled with conventional antithrombotic agents.

Introduction

Protein disulfide isomerase (PDI) is the prototypical member of an extended family of oxidoreductases, best known as endoplasmic reticulum-resident enzymes. These enzymes catalyze posttranslational disulfide bond formation and exchange and serve as chaperones during protein folding (1). Despite having a C-terminal endoplasmic reticulum retention sequence, PDI has been identified at many diverse subcellular locations outside the endoplasmic reticulum. It has biological functions on the cell surfaces of lymphocytes, hepatocytes, platelets, and endothelial cells (2–6). Platelets are a rich source of extracellular PDI, expressing this protein on their surface and also secreting PDI in response to thrombin stimulation (5, 7). Endothelial cells also express PDI upon agonist stimulation or when challenged by a vascular injury (3, 8).

We have previously shown that PDI is rapidly secreted from both endothelial cells and platelets during thrombus formation in vivo (7, 8). Inhibition of PDI using neutralizing antibodies blocks thrombus formation in several thrombosis models (refs. 6–9 and L. Bellido-Martin, B. Furie, B.C. Furie, unpublished observations). Inhibition of PDI in these models abrogates not only platelet accumulation at the injury site but also fibrin generation (7, 8). These observations demonstrate a critical role for extracellular PDI in the initiation of thrombus formation.

The potent antithrombotic activity of neutralizing antibodies directed at PDI indicates that PDI could be a useful target in the pharmacological control of thrombus formation. However, potential complications of inhibiting PDI are the ubiquitous distribution and critical function of intracellular PDI. Chronic PDI silencing is toxic in cultured cells (10), and PDI-deficient animals have not been developed. In addition, presently available inhibitors of PDI are sulfhydryl-reactive compounds that bind covalently at the CXXC catalytic site (11); are nonselective, acting broadly on thiol isomerases (12); or are cytotoxic (13, 14). Identification of new small molecules that interfere with PDI activity but are otherwise nontoxic is required to test the feasibility of targeting PDI for inhibition of thrombus formation.

To identify antithrombotic PDI inhibitors, we screened a small molecule library enriched for bioactive compounds. This screen identified quercetin-3-rutinoside as a selective inhibitor of PDI activity. Quercetin-3-rutinoside is a flavonol abundant in a variety of commonly ingested foods. We found that quercetin-3-rutinoside inhibited thrombus formation at concentrations that are well tolerated in mice and humans. Inhibition of thrombus formation by quercetin-3-rutinoside in mice was completely reversed by infusion of recombinant PDI. These findings demonstrate the feasibility of targeting PDI for inhibition of thrombus formation.

Results

Identification of quercetin-3-rutinoside as a potent PDI inhibitor. We used an insulin-based turbidimetric assay modified for high-throughput screening to identify potent and selective small molecule inhibitors of PDI (15). The assay demonstrated a signal/noise ratio of 116:1, a coefficient of variance of 4.6%, and a Z-factor of 0.83. We screened a library of 4,900 compounds, including approximately 3,000 known bioactive compounds (Figure 1A). The screen identified 18 inhibitory compounds representative of 13 separate chemical scaffolds, including 3 flavonols. Flavonols are widely distributed plant polyphenolic compounds enriched in commonly ingested foods, such as buckwheat, berries, tea, and vegetables. Of the flavonols that we identified, quercetin-3-rutinoside (also known as rutin), a quercetin that is glycosylated at position 3 of the pyrone ring (C ring, Figure 2), was the most potent PDI inhibitor. Quercetin-3-rutinoside inhibited PDI in a dose-dependent manner with

Conflict of interest: The authors have declared that no conflict of interest exists.
Citation for this article: *J Clin Invest.* 2012;122(6):2104–2113. doi:10.1172/JCI61228.

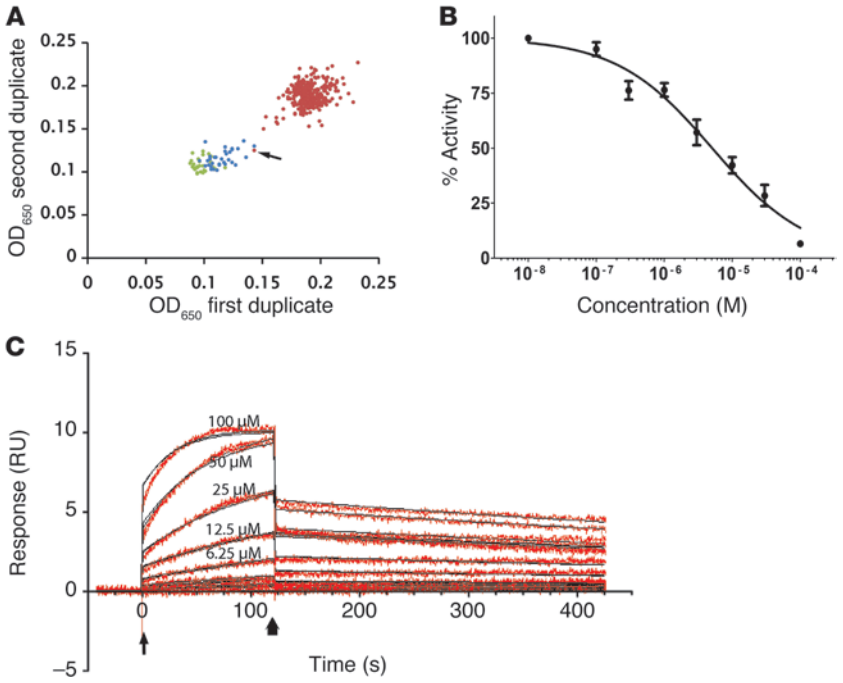

Figure 1

Identification of quercetin-3-rutinoside as a PDI inhibitor. (**A**) Data from representative 384-well plates, including samples with no PDI (green); 3 mM bacitracin, a nonspecific inhibitor of the PDI family of oxidoreductases (blue); or test compounds (red). Duplicate readings are plotted, and an arrow indicates the inhibitory compound identified as quercetin-3-rutinoside. Each symbol represents an individual reading. (**B**) Effect of the indicated concentrations of quercetin-3-rutinoside on PDI activity, determined using the insulin reduction assay (mean ± SD). (**C**) Sensorgram of binding of quercetin-3-rutinoside to recombinant PDI. The thin arrow indicates the time of injection of quercetin-3-rutinoside onto the PDI-coated sensor chip, and the thick arrow indicates the time of injection of regeneration buffer. Black lines represent the fitted curves for duplicates of the varying concentrations of quercetin-3-rutinoside analyte at 0, 0.39, 0.78, 1.56, 3.13, 6.25, 12.5, 25, 50, and 100 μM.

an IC_{50} of 6.1 μM (1.1–10.7 μM, 95% confidence interval) (Figure 1B and Supplemental Figure 1A; supplemental material available online with this article; doi:10.1172/JCI61228DS1). Inhibition of PDI by quercetin-3-rutinoside was confirmed in a fluorescence-based reductase assay using oxidized glutathione coupled to di-eosin (Di-E-GSSG) (ref. 16 and data not shown). PDI inhibition by quercetin-3-rutinoside was fully and rapidly reversible (Supplemental Figure 1B), indicating that quercetin-3-rutinoside does not covalently bind PDI. Evaluation of quercetin-3-rutinoside binding to immobilized PDI using surface plasmon resonance indicated a K_d of 2.8 μM (Figure 1C).

Quercetin-3-rutinoside is a selective inhibitor of PDI. Several thiol reductases have been identified in vascular cells and may be released into the extravascular space. To evaluate the selectivity of quercetin-3-rutinoside for PDI, we determined its activity against other oxidoreductases (1) known to be secreted from platelets or endothelial cells (17). Quercetin-3-rutinoside failed to inhibit ERp5, ERp57, ERp72, thioredoxin (Figure 3A), or thioredoxin reductase (Figure 3B). These oxidoreductases share with PDI the active-site motif CGHC and display reductase activity similar to that of PDI. However, even at 30 μM, quercetin-3-rutinoside had negligible inhibition (~10%) of other oxidoreductases. Thus, quercetin-3-rutinoside binds to and reversibly inhibits PDI but shows only minimal activity toward other extracellular thiol isomerases present in the vasculature.

Quercetin-3-rutinoside analogs as PDI inhibitors. Ingested quercetin-3-rutinoside is hydrolyzed to quercetin in the intestine and further modified to other conjugated metabolites of quercetin (18). We evaluated the ability of common metabolites of quercetin-3-rutinoside and other analogs to inhibit PDI activity. Quercetin-3-glucuronide, one of the abundant quercetin-3-rutinoside metabolites found in plasma, demonstrated an IC_{50} of 5.9 μM (3.5–10.1 μM, 95% confidence interval). Isoquercetin, hyperoside, and datiscin, all of which have a 3-O-glycosidic linkage (Figure 2), also inhibited PDI reductase activity. The inhibitory activity of these compounds was similar irrespective of the nature of glycoside in the 3 position on ring C or the substituents on ring B. In contrast, metabolites that lack a 3-O-glycoside, such as tamarixetin, isorhamnetin, diosmetin, or quercetin, did not inhibit PDI reductase activity, whether or not they were hydroxylated or methoxylated at the 3′ and 4′ positions on ring B (Figure 2). These studies show that the inhibitory activity against PDI for this group of flavonols is restricted to those with a 3-O-glycoside linkage.

Quercetin-3-rutinoside inhibits platelet aggregation and endothelial cell–mediated fibrin generation in vitro. Antibody-mediated inhibition of PDI blocks platelet aggregation in vitro (2, 4, 5). Quercetin-3-rutinoside has previously been demonstrated to inhibit platelet aggregation induced by collagen or ADP (19, 20). In anticipation of in vivo thrombus formation studies in mice, we evaluated the effect of quercetin-3-rutinoside on PAR4-mediated platelet aggregation. We have previously demonstrated that PAR4-mediated platelet activation is required for thrombus formation in vivo in mice (21). Quercetin-3-rutinoside inhibited aggregation of washed human platelets induced by the PAR4 peptide agonist AYPGKF (Figure 4A). Inhibition of platelet aggregation by quercetin-3-rutinoside was completely reversed when platelets incubated with quercetin-3-rutinoside were washed prior to stimulation with AYPGKF (Figure 4B). When quercetin-3-rutinoside was infused into mice, platelet-rich plasma obtained from mice demonstrated reduced aggregation in response to AYPGKF compared with that of mice infused with vehicle alone (Figure 4C). These studies indicate that the antiplatelet effect of quercetin-3-rutinoside is maintained after infusion.

PDI is released from HUVECs after laser-mediated activation (8). When incubated in plasma, these activated HUVECs generate fibrin. Inhibition of PDI blocks fibrin generation in this assay (8). Incubation of HUVECs with quercetin-3-rutinoside prior to laser-mediated activation resulted in a significant reduction in fibrin formation (Figure 5, A and B). However, cell activation, as measured by intracellular calcium mobilization after laser stimulation, was comparable in quercetin-3-rutinoside–treated or buffer-treated endothelial cells (Supplemental Figure 2). Thus, quercetin-3-rutinoside blocked fibrin generation at a step distal to endothelial cell activation and calcium mobilization. The inhibitory effect of quercetin-3-rutinoside on fibrin generation was dose dependent, with an IC_{50} of approximately 5 μM querce-

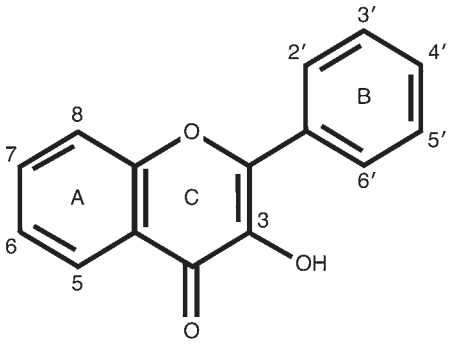

Name	2′	3′	4′	5′	3	IC_{50} (μM) (95% confidence interval)
Quercetin	H	OH	OH	H	OH	>100
Tamarixetin	H	OH	OCH_3	H	OH	>100
Isorhamnetin	H	OCH_3	OH	H	OH	>100
Diosmetin	H	OH	OCH_3	H	H	>100
Hyperoside	H	OH	OH	H	Galactose	5.9 (2.8–12.5)
Isoquercetin	H	OH	OH	H	Glucose	7.1 (4.3–12.0)
Quercetin-3-glucuronide	H	OH	OH	H	Glucuronic acid	5.9 (3.5–10.1)
Quercetin-3-rutinoside	H	OH	OH	H	Rutinose	6.1 (1.1–10.7)
Datiscin	OH	H	H	H	Rutinose	8.8 (3.2–24.3)

Figure 2
Structure-activity relationship of the flavonols and their potency (IC_{50}) of PDI inhibition. Numbers in structure correspond with those in the column headings.

tin-3-rutinoside and 95% reduction in fibrin at 10 μM quercetin-3-rutinoside ($P < 0.001$) (Figure 5). Similar inhibition of fibrin generation was observed in the presence of a function blocking PDI antibody (Figure 5C). Thus, quercetin-3-rutinoside inhibits both platelet aggregation and fibrin generation in vitro.

Quercetin-3-rutinoside inhibits thrombus formation in vivo. Inhibition of extracellular PDI by neutralizing antibodies blocks thrombus formation in several mouse thrombosis models (7–9). To analyze the effect of quercetin-3-rutinoside on thrombus formation, we compared platelet accumulation and fibrin generation after laser injury of mouse cremaster arterioles (22). Intravenous infusion of quercetin-3-rutinoside resulted in a dose-dependent inhibition of platelet accumulation, with 71% reduction (measured by area under the curve) at 0.1 mg/kg quercetin-3-rutinoside (Figure 6, A–E). As observed with anti-PDI antibodies (7, 8), fibrin generation was inhibited after quercetin-3-rutinoside infusion, reduced to 68% of that of vehicle control with 0.3 mg/kg quercetin-3-rutinoside (Figure 6, A–D, and F). Both platelet accumulation and fibrin generation were nearly absent after infusion of 0.5 mg/kg quercetin-3-rutinoside. Quercetin-3-rutinoside also inhibited thrombus formation after $FeCl_3$ injury. Infusion of 0.5 mg/kg quercetin-3-rutinoside resulted in a 2.2-fold increase ($P = 0.003$) in occlusion time after exposure of cremaster arterioles to $FeCl_3$ (Figure 6G). This result indicates that the protective effect of quercetin-3-rutinoside during thrombus formation is not model specific.

Since quercetin-3-rutinoside is incompletely absorbed and extensively metabolized after ingestion, we evaluated the effect of quercetin-3-rutinoside administered by oral gavage to assess the antithrombotic potential of ingested quercetin-3-rutinoside and its metabolites in the thrombosis model. In this model, orally administered quercetin-3-rutinoside blocks platelet accumulation, with an IC_{50} of approximately 10 mg/kg quercetin-3-rutinoside (Figure 7A), and fibrin formation, with an IC_{50} of approximately 15 mg/kg quercetin-3-rutinoside (Figure 7B). Thus, quercetin-3-rutinoside is an antithrombotic in this model, regardless of the route of administration. Plasma levels of quercetin-3-rutinoside decrease rapidly after either intravenous or oral administration (Supplemental Table 1). Given the extensive metabolism of quercetin-3-rutinoside, it is possible that metabolites contribute to its antithrombotic activity in vivo.

PDI is the target of quercetin-3-rutinoside inhibition of thrombus formation in vivo. To evaluate the selectivity of PDI inhibition by quercetin-3-rutinoside during thrombus formation, the antithrombotic activity of diosmetin was evaluated in the thrombosis model. Diosmetin lacks a hydroxyl group at position 3 of the C ring and cannot undergo glycosylation at this position (Figure 2). Consistent with its inability to block PDI activity in vitro, diosmetin had no significant effect on either platelet accumulation or fibrin generation after laser-induced vascular injury (Figure 8). Pharmacokinetic studies demonstrate that diosmetin is cleared more slowly than quercetin-3-rutinoside (23). Thus, the lack of effect of diosmetin on thrombus formation compared with that of quercetin-3-rutinoside is not secondary to rapid elimination or metabolism. This result demonstrates that a structurally related flavonol that lacks PDI inhibitory activity fails to block thrombus formation in vivo.

We then examined the ability of infused exogenous recombinant PDI to overcome the inhibitory effect of quercetin-3-rutinoside on

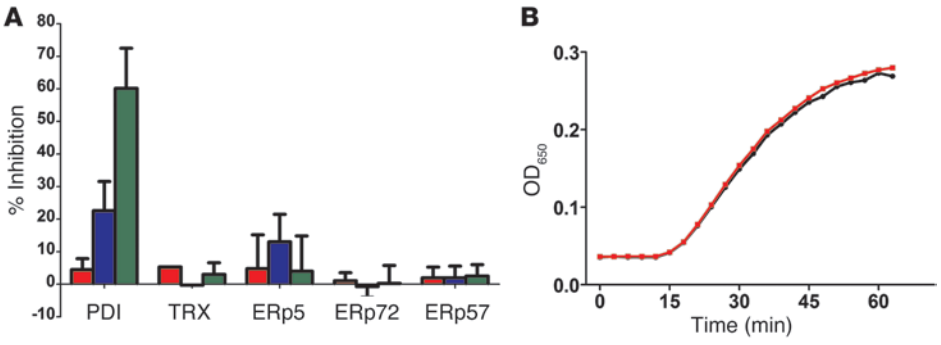

Figure 3
Quercetin-3-rutinoside selectively inhibits PDI. (**A**) Effect of quercetin-3-rutinoside at 0.3 μM (red), 3 μM (blue), and 30 μM (green) on PDI, thioredoxin (TRX), ERp5, ERp72, and ERp57 activity, as measured in the insulin reduction assay. Data show the mean and SD of 3 independent determinations. (**B**) Insulin reductase assay in the absence (black) or presence (red) of 30 μM quercetin-3-rutinoside in addition to thioredoxin, thioredoxin reductase, and NADPH as reducing equivalent.

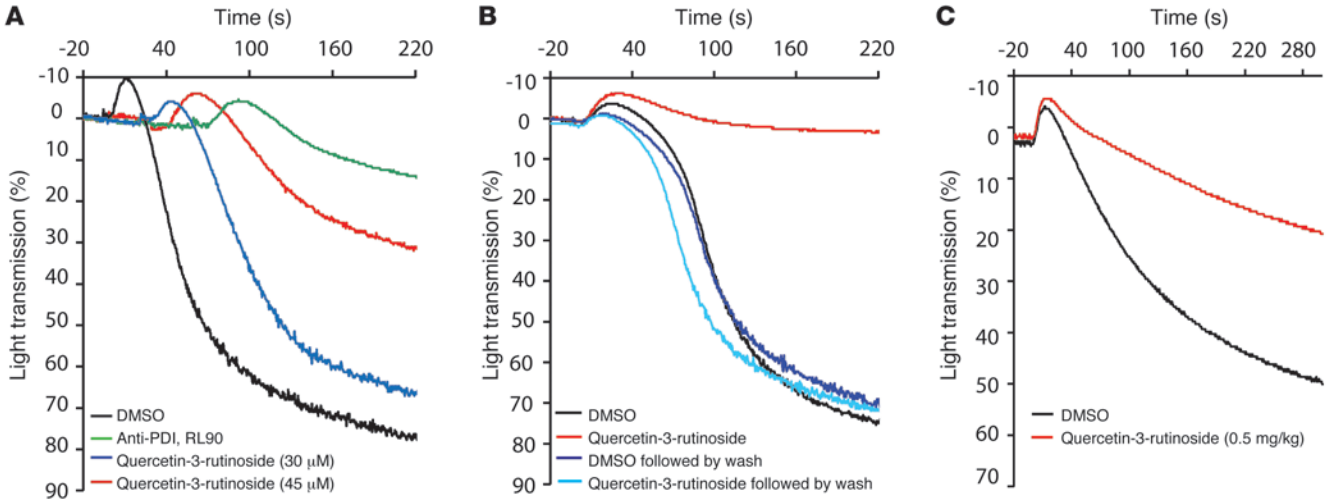

Figure 4

Quercetin-3-rutinoside inhibits platelet aggregation. (**A**) Washed human platelets (2×10^8 platelets/ml) were incubated with vehicle alone (black), 30 μM quercetin-3-rutinoside (blue), 45 μM quercetin-3-rutinoside (red), or anti-PDI antibody, RL90 (green), for 15 minutes and subsequently stimulated with 50 μM PAR4 peptide AYPGKF. (**B**) Washed human platelets (2×10^8 platelets/ml) were incubated with either vehicle (black) or 60 μM quercetin-3-rutinoside (red) for 15 minutes or incubated with vehicle followed by a wash (dark blue) or 60 μM quercetin-3-rutinoside followed by a wash (light blue) and subsequent stimulation with 50 μM PAR4 peptide AYPGKF. (**C**) Quercetin-3-rutinoside was infused into mice intravenously at 0.5 mg/kg. Five minutes after infusion, blood was obtained by cardiac puncture, and platelet-rich plasma was isolated. Platelet-rich plasma from quercetin-3-rutinoside–treated mice (red) or vehicle control (black) was stimulated with 200 μM AYPGKF.

thrombus formation. Mice were infused with quercetin-3-rutinoside or vehicle, and then half the mice in each group were infused with a bolus of recombinant PDI prior to laser injury (Figure 9). As before, quercetin-3-rutinoside infusion resulted in reduction of platelet accumulation (Figure 9, B and E) and fibrin deposition (Figure 9, B and F). This effect was completely reversed in mice that received an infusion of exogenous recombinant PDI (Figure 9, C, E, and F). Infusion of exogenous PDI in the absence of prior infusion of quercetin-3-rutinoside did not significantly affect thrombus size or fibrin generation relative to those in untreated mice (Figure 9, D–F). These results demonstrate that the amount of PDI released by endothelial cells and platelets upon cell activation at the site of injury is sufficient to generate a maximal thrombotic response to the stimulus. They further support the interpretation that impairment of thrombus formation in vivo by quercetin-3-rutinoside is mediated via inhibition of PDI.

Discussion

The identification of quercetin-3-rutinoside as an antagonist of PDI and an inhibitor of thrombus formation validates PDI as a drug target for antithrombotic therapy. Inhibition of PDI using neutralizing antibodies blocks thrombus formation in vivo after carotid artery ligation (9), ferric chloride exposure (unpublished observations, L. Bellido-Martin, B. Furie, and B.C. Furie), or laser injury (7, 8), demonstrating an essential role for PDI in thrombus formation in multiple models. This observation raises the question of whether small molecule inhibition of PDI could be used to control thrombus formation in vivo, particularly given the advantage that both platelet accumulation and fibrin generation are blocked following inhibition of PDI. Several observations indicated that PDI is the relevant molecular target of quercetin-3-rutinoside in our thrombus formation studies. Quercetin-3-rutinoside selectively inhibited PDI, without significant inhibition of other thiol isomerases that may

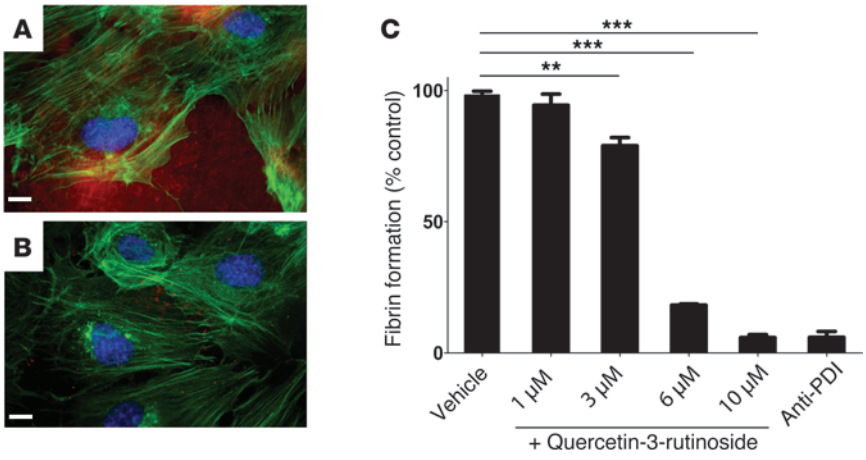

Figure 5

Quercetin-3-rutinoside inhibits fibrin generation in vitro. (**A** and **B**) Representative images of fixed and immunostained HUVECs that have been activated by laser injury in the presence of plasma and calcium (**B**) with or (**A**) without quercetin-3-rutinoside (10 μM). The cells were fixed after laser activation and stained for fibrin (red), FITC-phalloidin (green), and DAPI (blue). (**C**) Quantification of fibrin signal detected on cultured endothelial cells expressed as the percentage inhibition of fibrin after laser activation (mean ± SD). $^{**}P < 0.01$, $^{***}P < 0.001$. Original magnification, ×60. Scale bars: 10 μm.

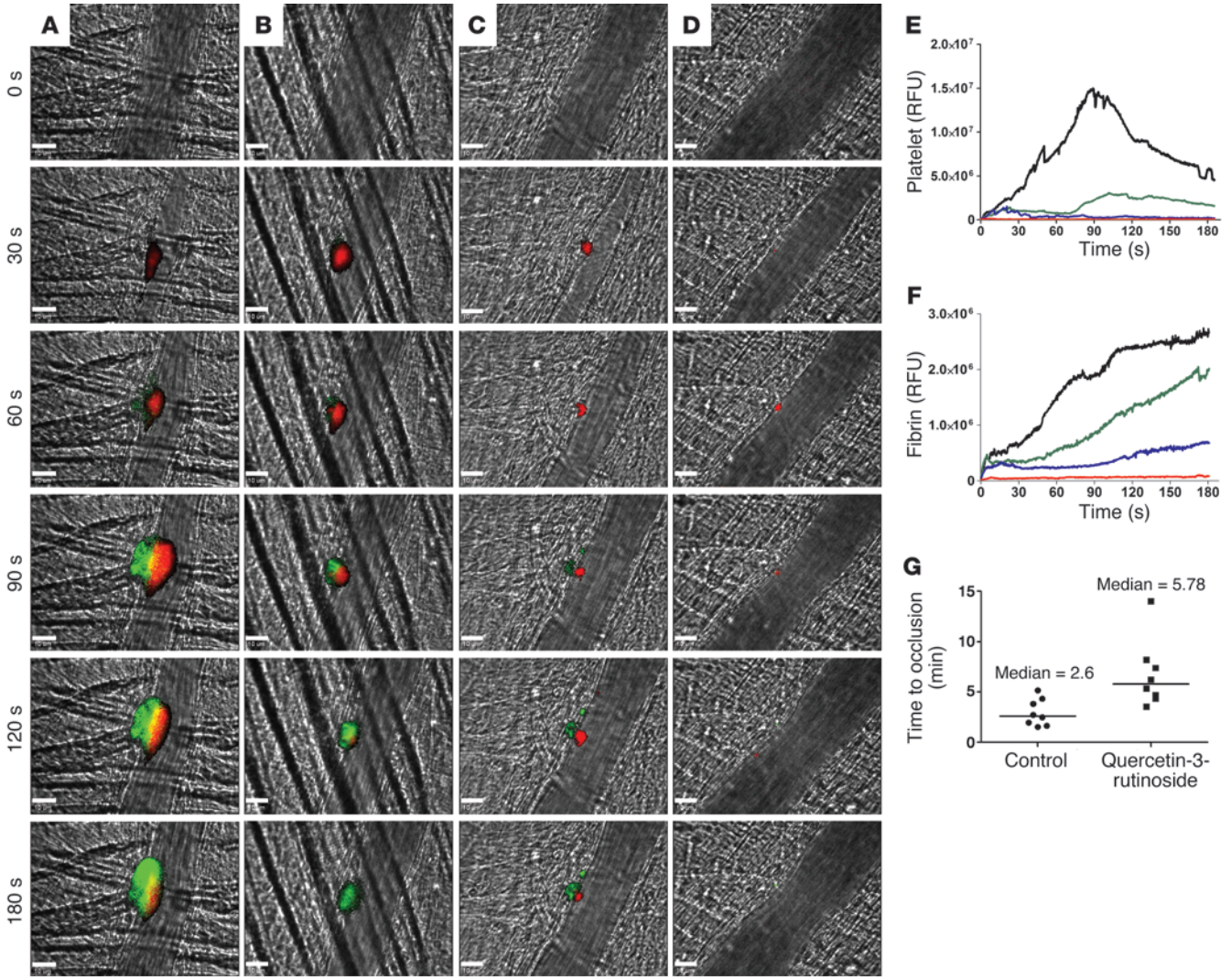

Figure 6

Quercetin-3-rutinoside inhibits thrombus formation and fibrin generation in vivo. Platelet-specific anti-CD42b antibody conjugated to Dylight 649 (0.1 μg/g body weight) and fibrin-specific mouse anti-human fibrin II β-chain monoclonal antibody conjugated to Alexa Fluor 488 (0.5 μg/g body weight) were infused into the mice. At varying doses, quercetin-3-rutinoside was subsequently infused intravenously 5 minutes prior to the initial laser injury. Representative binarized images of the appearance of fluorescence signals associated with fibrin (green) and platelets (red) over the 180 seconds after laser-induced vessel wall injury in wild-type mice are shown in **A**–**D**, with mice infused with (**A**) vehicle only; (**B**) quercetin-3-rutinoside at 0.1 mg/kg body weight; (**C**) quercetin-3-rutinoside at 0.3 mg/kg body weight; and (**D**) quercetin-3-rutinoside at 0.5 mg/kg body weight shown. (**E**) Median integrated platelet fluorescence intensity and (**F**) median integrated fibrin fluorescence intensity at the injury site are plotted versus time, with mice infused with vehicle only (black); quercetin-3-rutinoside at 0.1 mg/kg body weight (green); quercetin-3-rutinoside at 0.3 mg/kg body weight (blue); and quercetin-3-rutinoside at 0.5 mg/kg body weight shown (red). Data are from 30 thrombi in 3 mice for each condition. RFU, relative fluorescence units. (**G**) Quercetin-3-rutinoside at 0.5 mg/kg was infused 5 minutes prior to $FeCl_3$ injury of cremaster arterioles. Data points represent time to occlusion, as determined by cessation of flow in control mice infused with vehicle or mice infused with quercetin-3-rutinoside as indicated. Horizontal bars denotes median values. Original magnification, ×60. Scale bars: 10 μm.

have been present in the vasculature during thrombus formation. A structurally related analog of quercetin-3-rutinoside, diosmetin, which does not inhibit PDI, failed to inhibit thrombus formation. In addition, the antithrombotic activity of quercetin-3-rutinoside was entirely reversed after infusion of recombinant PDI. Thus, although quercetin-3-rutinoside may have other physiologic properties, the dominant effect of quercetin-3-rutinoside in thrombus formation is to inhibit extracellular PDI function, thereby preventing thrombi from forming after vascular injury.

PDI inhibition prevents both platelet accumulation and fibrin generation during thrombus formation. Although the substrates activated by PDI during thrombus formation remain unknown, candidates have been proposed. PDI has been implicated in $\alpha_{IIb}\beta_3$-mediated platelet aggregation (2, 24). Antibodies directed at PDI inhibit platelet aggregation in vitro (4), and this effect has been attributed in part to the influence of PDI on $\alpha_{IIb}\beta_3$ conformation (4, 25). Glycoprotein $1b_\alpha$ contains free thiols and is modified by PDI (5). PDI catalyzed disulfide exchange also influences adhesion

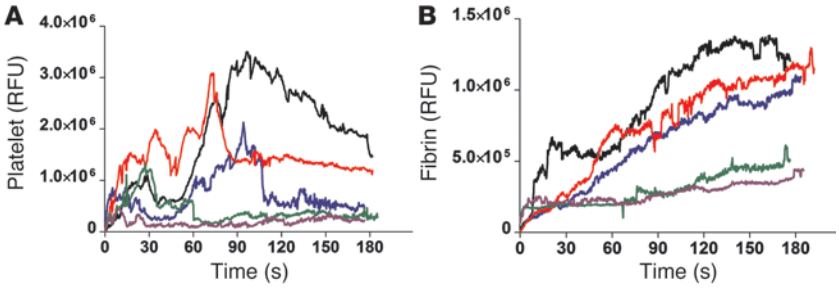

Figure 7

Oral quercetin-3-rutinoside inhibits thrombus formation and fibrin generation in vivo. Platelet-specific anti-CD42b antibody conjugated to Dylight 649 (0.1 μg/g body weight) and fibrin-specific mouse anti-human fibrin II β-chain monoclonal antibody conjugated to Alexa Fluor 488 (0.5 μg/g body weight) were infused into the mice. (**A**) Median integrated platelet fluorescence and (**B**) fibrin fluorescence at the injury site after oral gavage with quercetin-3-rutinoside 90 minutes prior to injury are plotted versus time, with mice gavaged with vehicle only (black); with 5 mg/kg quercetin-3-rutinoside (red); with 10 mg/kg quercetin-3-rutinoside (blue); with 20 mg/kg quercetin-3-rutinoside (green); and with 50 mg/kg quercetin-3-rutinoside (purple). Data are from 30 thrombi in 3 mice for each condition.

of collagen to $\alpha_2\beta_1$ (26). Quercetin-3-rutinoside inhibited platelet aggregation in vitro. Moreover, platelet-rich plasma from mice infused with quercetin-3-rutinoside demonstrated impaired aggregation compared with platelet-rich plasma from control mice when tested ex vivo (Figure 4C), indicating that the compound directly impairs platelet aggregation. The direct effect of quercetin-3-rutinoside on platelet receptors in vivo, however, remains to be determined.

Fibrin formation after laser-induced injury of arterioles occurs in a platelet-independent manner, and the endothelium is an important source of PDI during thrombus formation (8, 27). Previous studies using cultured endothelial cells demonstrate that fibrin formation is dependent on endothelial cell–derived PDI (8). We found that quercetin-3-rutinoside inhibited fibrin formation on cultured endothelial cells with approximately the same potency as it inhibited purified PDI in the insulin reductase assay. Quercetin-3-rutinoside failed to inhibit endothelial cell activation (Supplemental Figure 2, A–C), and it did not inhibit fibrin formation induced by thrombin (Supplemental Figure 2D). These observations are consistent with an effect of quercetin-3-rutinoside on PDI. The relevant PDI substrates on endothelium are not known. Thiol isomerase–catalyzed oxidation of an allosteric disulfide bond in tissue factor may convert it from a noncoagulant cryptic state to a procoagulant decrypted state by PDI-mediated oxidation (28–30). However, the role of PDI in tissue factor deencryption is controversial and indirect pathways have been proposed (31). $\alpha_v\beta_3$ is also a putative PDI substrate on endothelial cells (32), though its role in thrombus formation is not known. Alternatively, extracellular PDI has been invoked in a transnitrosation reaction, enabling delivery of nitric oxide from extracellular to intracellular environments (33).

The observation that a commonly ingested flavonol and its metabolites are potent inhibitors of PDI indicates the feasibility of targeting PDI without substantial toxicity. Genetic deletion of PDI is toxic to cells (10, 34). The fundamental role of PDI in disulfide bond formation and protein folding raises the question of whether PDI inhibition can be well tolerated. We found that quercetin-3-rutinoside demonstrates no toxicity in cultured endothelial cells for at least 72 hours at concentrations as high as 100 μM quercetin-3-rutinoside (data not shown). Quercetin-3-rutinoside may lack toxicity because the same glycosidic linkage that is required for inhibition of PDI activity impairs cell permeability. Thus, flavonols with 3-O-glycosidic linkages could preferentially target extracellular PDI.

Plasma concentrations of quercetin-3-rutinoside achieved after infusion during thrombus formation studies were substantially lower than concentrations required for inhibition of PDI in vitro. Quercetin-3-rutinoside concentrations detected in vivo were also lower than those required for inhibition of platelet aggregation or fibrin generation on endothelial cells. Several considerations limit the strength of conclusions that can be drawn from a comparison of in vitro and in vivo findings. Foremost among these is the extensive metabolism of quercetin-3-rutinoside in vivo. Exposure to quercetin-3-rutinoside results in the generation of more than 60 metabolites (35). Many major metabolites, such as quercetin-3-glucuronide, possess a 3-O-glycosidic linkage and are active against PDI, as demonstrated by structure activity relationships (Figure 2). In addition, rutinosides are known to bind to the blood vessel wall (36, 37), where they may maintain antithrombotic activity but not be detected in plasma. Also limiting comparisons between in vitro studies of purified PDI and in vivo studies is the fact that in vitro studies rely on reduction of insulin by PDI while the relevant PDI substrates during thrombus formation in vivo remain to be determined. Thus, while these data are consistent with the possibility that quercetin-3-rutinoside is more potent in vivo than in vitro, it is difficult to draw firm conclusions regarding such a comparison.

Quercetin-3-rutinoside and the other 3-O-glycoside–linked flavonols identified as PDI inhibitors are found in high concentrations in tea, fruits, berries, and buckwheat (38). Multiple studies demonstrate that chronic administration of dietary flavonols, at concentrations as high as 3,000 mg/kg, has no significant toxicity in animal studies (39–41). Dietary flavonols used in clinical trials have also been well tolerated (41). Epidemiologic studies evaluating the effect of flavonol ingestion on cardiovascular events demonstrate protection from myocardial infarction and stroke with increased intake (42–44).

In summary, we identify quercetin-3-rutinoside as an inhibitor of PDI and show that inhibition of PDI potently blocks thrombus formation in vivo. These observations provide proof of principle for targeting extracellular PDI for inhibition of thrombus formation. Other agents that inhibit PDI function, such as juniferdin (14) or bacitracin (45), also inhibit thrombus formation in vivo (data not shown and ref. 7). However, these agents are either cytotoxic or nonselective (12, 14). The fact that quercetin-3-rutinoside is antithrombotic at flavonol concentrations that are well tolerated, based on extensive animal and human clinical literature, indicates that inhibition of extracellular PDI is a safe strategy for inhibition of thrombus formation. Pharmacological regulation of PDI enzymatic activity could prevent thrombosis in the setting of coronary artery disease, stroke, or venous thromboembolism.

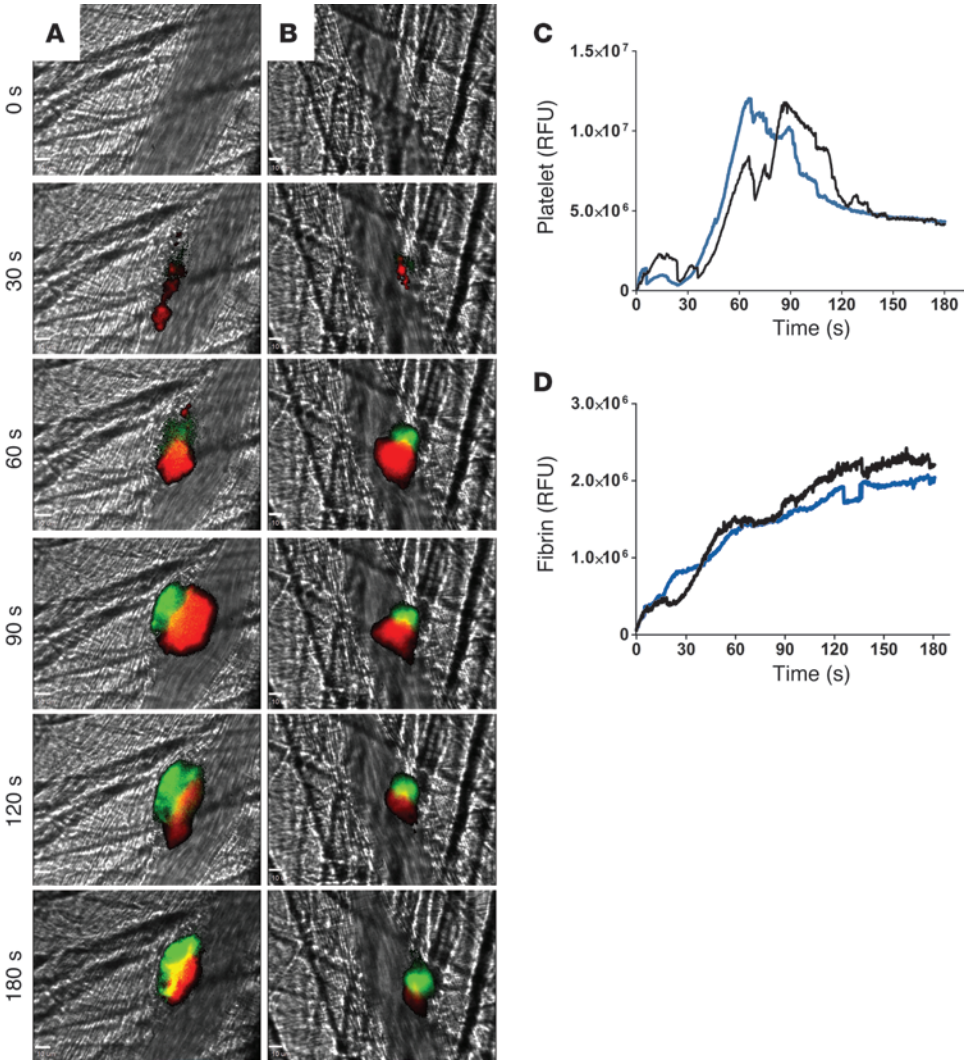

Figure 8
The quercetin analog diosmetin does not affect thrombus formation and fibrin generation in vivo. Platelet-specific anti-CD42b antibody conjugated to Dylight 649 (0.1 μg/g body weight) and fibrin-specific mouse anti-human fibrin II β-chain monoclonal antibody conjugated to Alexa Fluor 488 (0.5 μg/g body weight) were infused into the mice. Diosmetin at 10 mg/kg body weight or vehicle control was subsequently infused intravenously immediately prior to the initial laser injury. Representative binarized images of the appearance of fluorescence signals associated with fibrin (green) and platelets (red) over 180 seconds after laser-induced vessel wall injury in a wild-type mouse are shown in **A** and **B**, with mice infused with (**A**) vehicle only or (**B**) diosmetin at 10 mg/kg body weight. (**C**) Median integrated platelet fluorescence intensity and (**D**) median integrated fibrin fluorescence intensity at the injury site are plotted versus time, with mice infused with vehicle only (black) or 10 mg/kg diosmetin (blue). Data are from 30 thrombi in 3 mice for each condition. Original magnification, ×60. Scale bars: 10 μm.

Methods

Animals. C57BL/6J mice were obtained from The Jackson Laboratory.

Antibodies and reagents. Antiplatelet antibody Dylight 649 CD42b was purchased from Emfret Analytics. Fluo-4 and protein G-Sepharose were purchased from Invitrogen. Quercetin-3-rutinoside, quercetin, isoquercetin, insulin, and PAR4 agonist peptide AYPGKF were purchased from Sigma-Aldrich. Quercetin-3-glucuronide was from Extrasynthese. All other flavonols were purchased from Chromadex. The anti-PDI antibody RL90 and recombinant ERp57 protein were from Abcam, ERp72 was from Enzo Life Sciences, and thioredoxin-1 was from R&D Systems. HUVECs and growth medium EBM-2 and supplements were purchased from Lonza.

Protein isolation. Human recombinant His-tagged PDI was cloned into a pET-15b vector and transformed into *E. coli* Origami B (DE3) (EMD Chemicals). ERp5 was cloned into the pET-15b vector and transformed into *E. coli* Origami 2 (DE3) (EMD Chemicals). The recombinant proteins were soluble and isolated by affinity chromatography with a Ni-NTA column (Qiagen) for PDI and cobalt affinity chromatography (Pierce Biotechnology) for ERp5. PDI was further purified by gel filtration over Superdex 200 (GE Healthcare). Mouse anti-human fibrin II β-chain monoclonal antibody was purified over protein G-Sepharose (Invitrogen) from a 59D8 hybridoma cell line (46) and labeled with Alexa Fluor 488 (Invitrogen).

Insulin reduction assay. Reductase activity was assayed by measuring the PDI or other thiol isomerase–catalyzed reduction of insulin in the presence of DTT. The aggregation of reduced insulin chains was measured by absorption at 650 nm. The high-throughput screen was performed in a 384-well plate format and a volume of 30 μl in the presence of 0.3 mM DTT, 60 nM PDI, 0.4 μM insulin, and 2 mM EDTA in 100 mM potassium phosphate, pH 7.4, at 25°C. The reaction mixture for subsequent insulin reduction assays contained 100 mM potassium phosphate (pH 7.4), 0.75 mM DTT, 2 mM EDTA, 0.1 mM bovine insulin, and 0.8 μM purified human PDI in a total volume of 135 μl in a 96-well plate. Thioredoxin-1 was used at 3 μM, while ERp5, ERp57, and ERp72 were all used at 0.8 μM. The progress of the reaction was monitored for 30 minutes at 23°C. Quercetin-3-rutinoside or control buffer was added prior to the addition of enzyme at the concentrations indicated. PDI activity in the presence of compound was determined by the following formula: PDI activity (%) = $(OD[_{compound + PDI + DTT}] - OD[_{DTT}])/(OD[_{PDI + DTT}] - OD[_{DTT}]) \times 100\%$. Enzyme inhibition was determined by the following formula: enzyme inhibition = $(1 - [OD_{max\{compound + enzyme\}}/OD_{max\{buffer\ control + enzyme\}}])$. IC_{50} values were calculated using nonlinear regression analysis. Reversibility assays were performed as described in the Supplemental Methods.

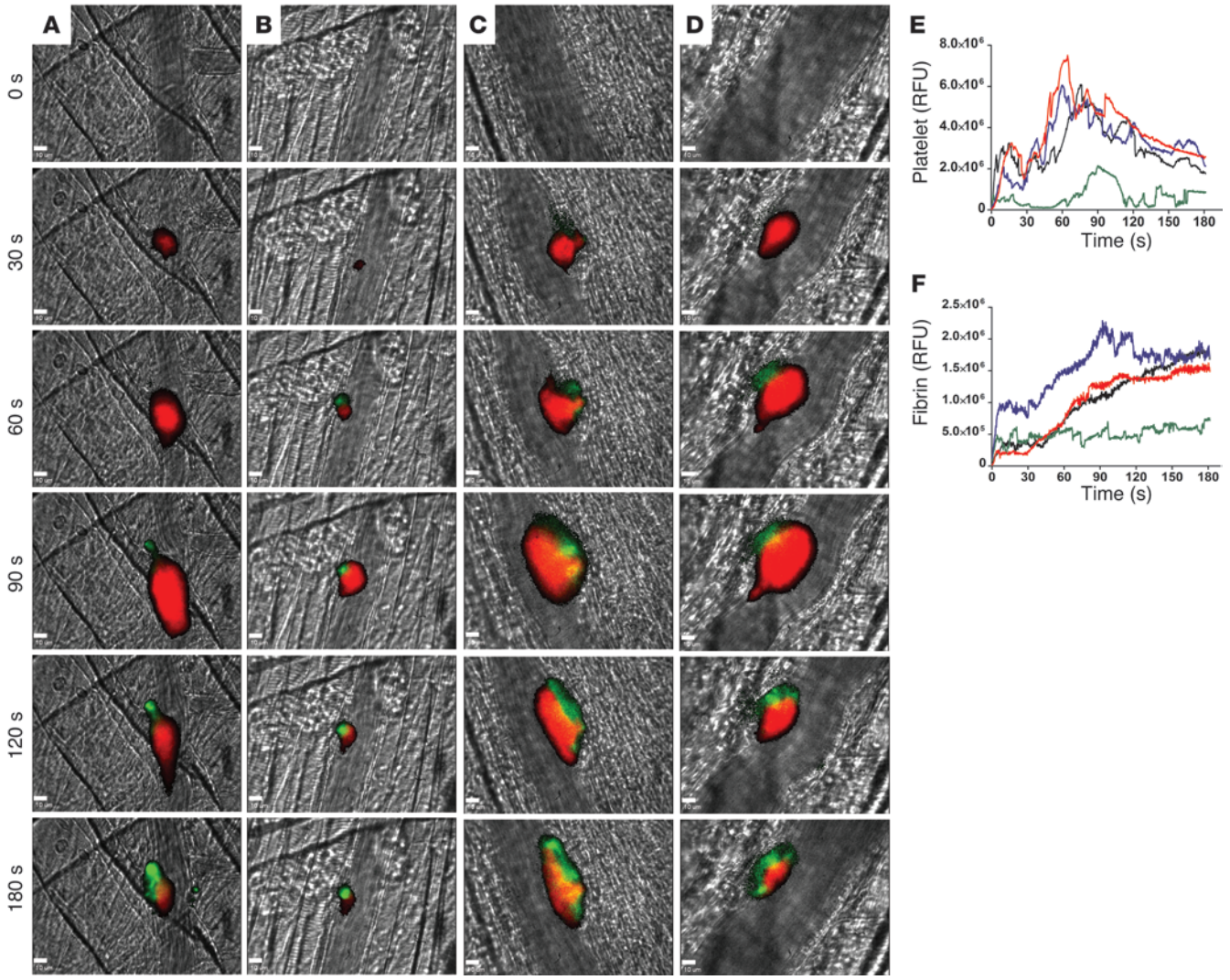

Figure 9

Exogenous PDI reverses quercetin-3-rutinoside inhibition of thrombus formation and fibrin generation in vivo. Dylight 649–conjugated anti-CD42b antibody and Alexa Fluor 488–conjugated fibrin-specific antibody were infused into mice. Mice were subsequently infused with (**A** and **D**) vehicle alone or (**B** and **C**) 0.25 mg/kg quercetin-3-rutinoside. After 6 to 12 initial thrombi, mice were infused with either (**A** and **B**) vehicle or (**C** and **D**) PDI at 200 μg per mouse to record additional thrombi. Representative binarized images of the appearance of fluorescence signals associated with fibrin (green) and platelets (red) over 180 seconds after laser-induced vessel wall injury. (**E**) Median integrated platelet fluorescence and (**F**) median integrated fibrin fluorescence at the injury site in mice infused with vehicle only (black), 0.25 mg/kg quercetin-3-rutinoside followed by vehicle (green), vehicle followed by 200 μg recombinant PDI (red), or 0.25 mg/kg quercetin-3-rutinoside followed by 200 μg recombinant PDI (blue). Data are from 30 thrombi in 3 mice for each condition. Original magnification, ×60. Scale bars: 10 μm.

Surface plasmon resonance. The interaction between PDI and quercetin-3-rutinoside was measured with a BIAcore T100 system (GE Healthcare) using PBS containing 0.005% P20 (GE Healthcare) and 0.5% DMSO. PDI in 10 mM sodium acetate (pH 5.5) was covalently coupled to a CM5 chip by amine coupling as per the manufacturer's instructions. A control surface underwent the same activation and deactivation in the absence of PDI. Quercetin-3-rutinoside solution at various concentrations was perfused over immobilized PDI at a flow rate of 95 μl per minute for 2 minutes followed by buffer alone, and the resonance changes were recorded. The sensorgram of the immobilized control surface was subtracted from that of the PDI-coated surface, and data were analyzed by BIAevaluation software (BIAcore, GE Healthcare).

Platelet aggregation. Washed human platelets (2×10^8 platelets/ml in Hepes-Tyrode buffer, 134 mM sodium phosphate, 2.9 mM KCl, 12 mM sodium bicarbonate, 20 mM HEPES, 1 mM magnesium chloride, 5 mM glucose [pH 7.3]) were incubated with the indicated concentrations of quercetin-3-rutinoside in PBS and 0.1% DMSO at 37°C for 15 minutes and then exposed to 50 μM PAR4 agonist AYPGKF. For studies of mouse platelets, mice were infused with quercetin-3-rutinoside (0.5 mg/kg) or vehicle alone. Five minutes after infusion, blood was obtained by cardiac puncture. Platelet-rich plasma was isolated by centrifugation at 200 *g* and evaluated for the aggregation in response to 200 μM AYPGKF. Aggregation was measured using a Chrono-Log 680 Aggregation System.

Endothelial cell stimulation and immunostaining. Endothelial cells were laser-activated as previously described (8, 47). Monolayers of HUVECs were cultured on 0.1% gelatin-coated photoetched coverslips (Bellco Glass) until they reached 80% confluence. Prior to laser stimulation, endothelial cells were loaded with Fluo-4. The cells were then immersed in recalcified plasma supplemented with corn trypsin inhibitor (100 μg/ml, Hematologic Technologies) and a specific PDI inhibitory antibody, RL90, or quercetin-3-rutinoside at various concentrations. Individual cells on the etched coverslip were activated with the Micropoint Laser System, and calcium mobilization was recorded. The reaction with plasma was stopped after 15 minutes with 20 mM EDTA, and the cells were immediately fixed in 3% paraformaldehyde for 5 minutes. After fixation, the cells were washed with PBS and stained with anti-fibrin antibody (clone 59D8) or an isotype-matched control antibody. Images were captured using a Roper CoolSNAP HQ camera. Thrombin-catalyzed fibrin polymerization assays were performed as described in the Supplemental Methods.

Intravital microscopy. Intravital video microscopy of the cremaster muscle microcirculation was performed as previously described (22). Digital images were captured with a Cooke Sensicam CCD camera (The Cooke Corporation) connected to a VS4-1845 Image Intensifier GEN III (Video Scope International).

Laser-induced injury. Injury to a cremaster arteriolar (30- to 50-μm diameter) vessel wall was induced with a Micropoint Laser System (Photonics Instruments) focused through the microscope objective, parfocal with the focal plane and tuned to 440 nm through the dye cell containing 5 mM coumarin in methanol (13). Data were captured digitally from 2 fluorescence channels, 488/520 nm and 647/670 nm. Data acquisition was initiated both prior to and after a single laser pulse for each injury. The microscope system was controlled and images were analyzed using Slidebook (Intelligent Imaging Innovations).

$FeCl_3$ injury. A paper filter saturated with 10% $FeCl_3$ was applied to the mouse cremaster muscle for 1 minute. The filter paper was removed, the tissue was washed using bicarbonate-buffered saline solution, and blood flow was evaluated by intravital microscopy. Time to occlusion was calculated from the time that the $FeCl_3$-saturated filter paper was removed from the tissue to the time that blood flow ceased.

Image analysis. For each thrombus generated by laser injury, a rectangular mask was defined that included a portion of the vessel upstream of the site of injury. The maximum fluorescence intensity of the pixels contained in this mask was extracted for all frames (before and after injury) for each thrombus. The mean value calculated from the maximal intensity values in the mask for each frame was determined and used as the background value. Finally, for each frame, the integrated fluorescence intensity was calculated as per following equation: integrated fluorescence intensity = sum Intensity of signal – (mean of the maximal background intensity × area of the signal). This calculation was performed for all frames in each thrombus and plotted versus time to provide the kinetics of thrombus formation (8, 27, 48, 49). For multiple fluorescence channels, calculations of background were made independently for each channel. The data from 25 to 30 thrombi were used to determine the median value of the integrated fluorescence intensity to account for the variability of thrombus formation in any given set of experimental conditions. Analysis of quercetin-3-rutinoside plasma levels was performed as described in the Supplemental Methods.

Statistics. A value representing area under the curve was calculated for each curve generated by measurement of fluorescence after laser injury of an arteriole. A Mann-Whitney test was used for statistical comparison of data sets comprised of 30 thrombi formed under each indicated condition. *P* values of 0.05 or less were considered statistically significant and are indicated. Statistical analyses were performed using Prism software package (version 4, GraphPad).

Study approval. The Beth Israel Deaconess Medical Center Institutional Animal Care and Use Committee approved all animal care and experimental procedures.

Acknowledgments

This work was supported by the NIH (grants HL087203, HL092125, and HL007917) and the American Heart Association (grant 0840043N). R. Jasuja and S.R. Bowley are recipients of American Heart Association grants (0825955D and 09POST2260692, respectively). F.H. Passam is a recipient of an International Exchange Award from the European Hematology Association–American Society of Hematology. L. van Hessem is supported in part by the Foundation for Women's Wellness.

Received for publication September 30, 2011, and accepted in revised form March 14, 2012.

Address correspondence to: Robert Flaumenhaft, Center for Life Science, Rm. 939, Beth Israel Deaconess Medical Center, 3 Blackfan Circle, Boston, Massachusetts 02215, USA. Phone: 617.735.4005; Fax: 617.735.4000; E-mail: rflaumen@bidmc.harvard.edu.

1. Hatahet F, Ruddock LW. Protein disulfide isomerase: a critical evaluation of its function in disulfide bond formation. *Antioxid Redox Signal*. 2009;11(11):2807–2850.
2. Manickam N, Sun X, Li M, Gazitt Y, Essex DW. Protein disulphide isomerase in platelet function. *Br J Haematol*. 2008;140(2):223–229.
3. Hotchkiss KA, Matthias LJ, Hogg PJ. Exposure of the cryptic Arg-Gly-Asp sequence in thrombospondin-1 by protein disulfide isomerase. *Biochim Biophys Acta*. 1998;1388(2):478–488.
4. Essex DW, Li M. Protein disulphide isomerase mediates platelet aggregation and secretion. *Br J Haematol*. 1999;104(3):448–454.
5. Burgess JK, et al. Physical proximity and functional association of glycoprotein 1balpha and protein-disulfide isomerase on the platelet plasma membrane. *J Biol Chem*. 2000;275(13):9758–9766.
6. Bennett TA, Edwards BS, Sklar LA, Rogelj S. Sulfhydryl regulation of L-selectin shedding: phenylarsine oxide promotes activation-independent L-selectin shedding from leukocytes. *J Immunol*. 2000;164(8):4120–4129.
7. Cho J, Furie BC, Coughlin SR, Furie B. A critical role for extracellular protein disulfide isomerase during thrombus formation in mice. *J Clin Invest*. 2008;118(3):1123–1131.
8. Jasuja R, Furie B, Furie BC. Endothelium-derived but not platelet-derived protein disulfide isomerase is required for thrombus formation in vivo. *Blood*. 2010;116(22):4665–4674.
9. Reinhardt C, et al. Protein disulfide isomerase acts as an injury response signal that enhances fibrin generation via tissue factor activation. *J Clin Invest*. 2008;118(3):1110–1122.
10. Hashida T, Kotake Y, Ohta S. Protein disulfide isomerase knockdown-induced cell death is cell-line-dependent and involves apoptosis in MCF-7 cells. *J Toxicol Sci*. 2011;36(1):1–7.
11. Mandel R, Ryser HJ, Ghani F, Wu M, Peak D. Inhibition of a reductive function of the plasma membrane by bacitracin and antibodies against protein disulfide-isomerase. *Proc Natl Acad Sci U S A*. 1993;90(9):4112–4116.
12. Karala AR, Ruddock LW. Bacitracin is not a specific inhibitor of protein disulfide isomerase. *FEBS J*. 2010;277(11):2454–2462.
13. Lovat PE, et al. Increasing melanoma cell death using inhibitors of protein disulfide isomerases to abrogate survival responses to endoplasmic reticulum stress. *Cancer Res*. 2008;68(13):5363–5369.
14. Khan MM, Simizu S, Lai NS, Kawatani M, Shimizu T, Osada H. Discovery of a small molecule PDI inhibitor that inhibits reduction of HIV-1 envelope glycoprotein gp120. *ACS Chem Biol*. 2011;6(3):245–251.
15. Smith AM, et al. A high-throughput turbidometric assay for screening inhibitors of protein disulfide isomerase activity. *J Biomol Screen*. 2004;9(7):614–620.
16. Raturi A, Mutus B. Characterization of redox state and reductase activity of protein disulfide isomerase under different redox environments using a sensitive fluorescent assay. *Free Radic Biol Med*. 2007;43(1):62–70.
17. Holbrook LM, Watkins NA, Simmonds AD, Jones CI, Ouwehand WH, Gibbins JM. Platelets release novel thiol isomerase enzymes which are recruited to the cell surface following activation. *Br J Haematol*. 2010;148(4):627–637.
18. Gee JM, DuPont MS, Day AJ, Plumb GW, Williamson G, Johnson IT. Intestinal transport of quercetin glycosides in rats involves both deglycosylation and interaction with the hexose transport pathway. *J Nutr*. 2000;130(11):2765–2771.
19. Sheu JR, Hsiao G, Chou PH, Shen MY, Chou DS. Mechanisms involved in the antiplate-

let activity of rutin, a glycoside of the flavonol quercetin, in human platelets. *J Agric Food Chem*. 2004;52(14):4414–4418.
20. Kim JM, Yun-Choi HS. Anti-platelet effects of flavonoids and flavonoid-glycosides from Sophora japonica. *Arch Pharm Res*. 2008;31(7):886–890.
21. Vandendries ER, Hamilton JR, Coughlin SR, Furie B, Furie BC. Par4 is required for platelet thrombus propagation but not fibrin generation in a mouse model of thrombosis. *Proc Natl Acad Sci U S A*. 2007;104(1):288–292.
22. Falati S, Gross P, Merrill-Skoloff G, Furie BC, Furie B. Real-time in vivo imaging of platelets, tissue factor and fibrin during arterial thrombus formation in the mouse. *Nat Med*. 2002;8(10):1175–1181.
23. Cova D, De Angelis L, Giavarini F, Palladini G, Perego R. Pharmacokinetics and metabolism of oral diosmin in healthy volunteers. *Int J Clin Pharmacol Ther Toxicol*. 1992;30(1):29–33.
24. Lahav J, Gofer-Dadosh N, Luboshitz J, Hess O, Shaklai M. Protein disulfide isomerase mediates integrin-dependent adhesion. *FEBS Lett*. 2000;475(2):89–92.
25. Essex DW, Li M, Miller A, Feinman RD. Protein disulfide isomerase and sulfhydryl-dependent pathways in platelet activation. *Biochemistry*. 2001;40(20):6070–6075.
26. Lahav J, et al. Enzymatically catalyzed disulfide exchange is required for platelet adhesion to collagen via integrin alpha2beta1. *Blood*. 2003; 102(6):2085–2092.
27. Bellido-Martin L, Chen V, Jasuja R, Furie B, Furie BC. Imaging fibrin formation and platelet and endothelial cell activation in vivo. *Thromb Haemost*. 2011;105(5):776–782.
28. Ahamed J, et al. Disulfide isomerization switches tissue factor from coagulation to cell signaling. *Proc Natl Acad Sci U S A*. 2006;103(38):13932–13937.
29. Chen VM, Ahamed J, Versteeg HH, Berndt MC, Ruf W, Hogg PJ. Evidence for activation of tissue factor by an allosteric disulfide bond. *Biochemistry*. 2006;45(39):12020–12028.
30. Chen VM, Hogg PJ. Allosteric disulfide bonds in thrombosis and thrombolysis. *J Thromb Haemost*. 2006;4(12):2533–2541.
31. Furlan-Freguia C, Marchese P, Gruber A, Ruggeri ZM, Ruf W. P2X7 receptor signaling contributes to tissue factor-dependent thrombosis in mice. *J Clin Invest*. 2011;121(7):2932–2944.
32. Swiatkowska M, Szymanski J, Padula G, Cierniewski CS. Interaction and functional association of protein disulfide isomerase with alphaVbeta3 integrin on endothelial cells. *FEBS J*. 2008;275(8):1813–1823.
33. Zai A, Rudd MA, Scribner AW, Loscalzo J. Cell-surface protein disulfide isomerase catalyzes transnitrosation and regulates intracellular transfer of nitric oxide. *J Clin Invest*. 1999;103(3):393–399.
34. Park B, et al. Redox regulation facilitates optimal peptide selection by MHC class I during antigen processing. *Cell*. 2006;127(2):369–382.
35. Olthof MR, Hollman PC, Buijsman MN, van Amelsvoort JM, Katan MB. Chlorogenic acid, quercetin-3-rutinoside and black tea phenols are extensively metabolized in humans. *J Nutr*. 2003; 133(6):1806–1814.
36. Neumann HA, Carlsson K, Brom GH. Uptake and localisation of O-(beta-hydroxyethyl)-rutosides in the venous wall, measured by laser scanning microscopy. *Eur J Clin Pharmacol*. 1992;43(4):423–426.
37. Patwardhan A, Carlsson K, Poullain JC, Taccoen A, Gerentes I. The affinity of troxerutin for the venous wall measured by laser scanning microscopy. *J Cardiovasc Surg (Torino)*. 1995;36(4):381–385.
38. Hollman PC, Hertog MG, Katan MB. Role of dietary flavonoids in protection against cancer and coronary heart disease. *Biochem Soc Trans*. 1996;24(3):785–789.
39. Carbonaro M, Grant G. Absorption of quercetin and rutin in rat small intestine. *Ann Nutr Metab*. 2005;49(3):178–182.
40. Ruiz MJ, et al. Dietary administration of high doses of pterostilbene and quercetin to mice is not toxic. *J Agric Food Chem*. 2009;57(8):3180–3186.
41. Harwood M, Danielewska-Nikiel B, Borzelleca JF, Flamm GW, Williams GM, Lines TC. A critical review of the data related to the safety of quercetin and lack of evidence of in vivo toxicity, including lack of genotoxic/carcinogenic properties. *Food Chem Toxicol*. 2007;45(11):2179–2205.
42. Hertog MG, Feskens EJ, Hollman PC, Katan MB, Kromhout D. Dietary antioxidant flavonoids and risk of coronary heart disease: the Zutphen Elderly Study. *Lancet*. 1993;342(8878):1007–1011.
43. Huxley RR, Neil HA. The relation between dietary flavonol intake and coronary heart disease mortality: a meta-analysis of prospective cohort studies. *Eur J Clin Nutr*. 2003;57(8):904–908.
44. Keli SO, Hertog MG, Feskens EJ, Kromhout D. Dietary flavonoids, antioxidant vitamins, and incidence of stroke: the Zutphen study. *Arch Intern Med*. 1996;156(6):637–642.
45. Dickerhof N, Kleffmann T, Jack R, McCormick S. Bacitracin inhibits the reductive activity of protein disulfide isomerase by disulfide bond formation with free cysteines in the substrate–binding domain. *FEBS J*. 2011;278(12):2034–2043.
46. Hui KY, Haber E, Matsueda GR. Monoclonal antibodies to a synthetic fibrin-like peptide bind to human fibrin but not fibrinogen. *Science*. 1983;222(4628):1129–1132.
47. Atkinson BT, Jasuja R, Chen VM, Nandivada P, Furie B, Furie BC. Laser-induced endothelial cell activation supports fibrin formation. *Blood*. 2010;116(22):4675–4683.
48. Celi A, et al. Thrombus formation: direct real-time observation and digital analysis of thrombus assembly in a living mouse by confocal and widefield intravital microscopy. *J Thromb Haemost*. 2003;1(1):60–68.
49. Dubois C, Atkinson B, Furie BC, Furie B. Real-time in vivo imaging of platelets during thrombus formation. In: Michelson AD, ed. *Platelets*. 2nd ed. New York, New York, USA: Elsevier; 2007:611–628.